Metabolomics (2013) 9:403–417
DOI 10.1007/s11306-012-0454-0

ORIGINAL ARTICLE

Investigating alginate production and carbon utilization in *Pseudomonas fluorescens* SBW25 using mass spectrometry-based metabolic profiling

Stina K. Lien · Håvard Sletta · Trond E. Ellingsen · Svein Valla · Elon Correa · Royston Goodacre · Kai Vernstad · Sven Even Finborud Borgos · Per Bruheim

Received: 10 March 2012 / Accepted: 15 August 2012 / Published online: 9 September 2012

Abstract Metabolic profiling of *Pseudomonas fluorescens* SBW25 and various mutants derived thereof was performed to explore how the bacterium adapt to changes in carbon source and upon induction of alginate synthesis. The experiments were performed at steady-state conditions in nitrogen-limited chemostats using either fructose or glycerol as carbon source. Carbon source consumption was up-regulated in the alginate producing mutant with inactivated anti-sigma factor MucA. The *mucA*- mutants (also non-alginate producing *mucA*- control strains) had a higher dry weight yield on carbon source implying a change in carbon and energy metabolism due to the inactivation of the anti-sigma factor MucA. Both LC–MS/MS and GC–MS methods were used for quantitative metabolic profiling, and major reorganization of primary metabolite pools in both an alginate producing and a carbon source dependent manner was observed. Generally, larger changes were observed among the phosphorylated glycolytic metabolites, the pentose phosphate pathway metabolites and the nucleotide pool than among amino acids and citric acid cycle compounds. The most significant observation at the metabolite level was the significantly reduced energy charge of the *mucA*- mutants (both alginate producing and non-producing control strains) compared to the wild type strain. This reduction was caused more by a strong increase in the AMP pool than changes in the ATP and ADP pools. The alginate-producing *mucA*- mutant had a slightly increased GTP pool, while the GDP and GMP pools were strongly increased compared to non-producing *mucA*- strains and to the wild type. Thus, whilst changes in the adenosine phosphate nucleotide pool are attributed to the *mucA* inactivation, adjustments in the guanosine phosphate nucleotide pool are consequences of the GTP-dependent alginate production induced by the *mucA* inactivation. This metabolic profiling study provides new insight into carbon and energy metabolism of the alginate producer *P. fluorescens*.

Keywords *Pseudomonas fluorescens* · Metabolic profiling · Mass spectrometry · Alginate synthesis · Anti-sigma factor MucA

Electronic supplementary material The online version of this article (doi:10.1007/s11306-012-0454-0) contains supplementary material, which is available to authorized users.

S. K. Lien · S. Valla · S. E. F. Borgos · P. Bruheim (✉)
Department of Biotechnology, Norwegian University of Science and Technology, Sem Sælands vei 6/8, 7491 Trondheim, Norway
e-mail: Per.Bruheim@biotech.ntnu.no

H. Sletta · T. E. Ellingsen · K. Vernstad · S. E. F. Borgos
Department of Biotechnology, SINTEF Materials and Chemistry, Trondheim, Norway

E. Correa · R. Goodacre
School of Chemistry, Manchester Institute of Biotechnology, University of Manchester, Manchester, UK

R. Goodacre
Manchester Centre for Integrative Systems Biology, Manchester Institute of Biotechnology, University of Manchester, Manchester, UK

1 Introduction

The polysaccharide alginate is composed of mannuronic acid and its C-5 epimer guluronic acid. Although, industrial production of the polymer is based on raw materials from seaweed, several bacteria also produce alginate and they are interesting producer organisms of polymannuronic acid. Polymannuronic acid can be used to tailor-make

alginate by post-synthesis enzymatic epimerase treatments (Rehm 2010), and thus studies of bacterial alginate synthesis are of importance for understanding and potential improvement of the bacterial alginate production process. Twenty-four genes have so far been found to be involved in alginate biosynthesis, of which 12 of the 13 structural genes are clustered in one operon under the control of a single promotor P_{algD} (Hay et al. 2010). The first gene in this operon is the GDP mannose dehydrogenase *algD*. The 13th structural gene *algC*, encodes phosphomannomutase, and is located outside the *alg* operon under the control of a separate promotor. Biosynthesis of alginate starts with conversion of fructose-6-phosphate (F6P) to mannose-6-phosphate (M6P) by AlgA, before further conversion to mannose-1-phosphate (M1P) by AlgC. M1P is then converted by the bifunctional enzyme AlgA to GDP-mannose (GDP-M), before GDP-M is further oxidized by AlgD to GDP-mannuronic acid (GDP-Mu), the direct precursor for polymerization. The remaining 10 structural genes take part in polymerization and modification of the polymer (a schematic overview of the biosynthesis of alginate alongside central metabolic pathways are given in Figs. 5 and 6). Several regulatory genes have also been identified to be involved in alginate biosynthesis, e.g. alginate synthesis is controlled by the anti-sigma factor MucA that binds the sigma factor AlgU preventing transcription of genes involved in alginate production (Martin et al. 1993; Schnider-Keel et al. 2001). Hence, wild-type *Pseudomonas fluorescens* does not produce alginate, whilst a *mucA* deficient mutant will. In fact *mucA* mutation is frequently associated with the mucoid phenotype of clinical *Pseudomonas aeruginosa* strains isolated from cystic fibrosis patients (Hassett et al. 2009). However, *mucA* deletion is expected to have other effects on *P. fluorescens* than initiation of alginate production. The reasons for this expectation is that AlgU is a global stress response sigma factor regulating several systems (Firoved and Deretic 2003).

Metabolomics, the comprehensive analysis of metabolite pools, can be very powerful for understanding metabolism in general (Villas-Boâs and Bruheim 2007; Wentzel et al. 2012), and for enhancing synthetic biology processes (Ellis and Goodacre 2012). However, when measuring many metabolites simultaneously one is faced with particular challenges due to the wide physiochemical properties of the different metabolite classes, ranging form hydrophilic and highly charged to hydrophobic metabolites. In addition, biological extracts might be quite complex and contain thousands of metabolites present at a wide range of concentrations. Mass spectrometry (MS) has become one dominant technology for detection and quantification of metabolites, and MS detection is especially sensitive and selective when hyphened to gas or liquid chromatography (GC and LC). For characterization of the hundred most abundant metabolites in an extract at least two to three targeted GC–MS and LC–MS methods need to be applied (van der Werf et al. 2007). Alternatively, non-targeted approaches using high mass accuracy MS instrumentation can be used, and several thousand metabolite features are usually detected. However, it is a tedious task to determine the identity of even the most abundant masses as there can be many metabolites with monoisotopic masses within the mass accuracy limits of the instrument. There are also many examples of metabolites with the same stoichiometric formula, thereby making a chromatographic step using metabolite standards necessary for exact identification (Sumner et al. 2007). Therefore, quantitative targeted methods are preferred as they yield data that can readily be interpreted in a biological context (Lu et al. 2008; Nielsen and Oliver 2005).

A metabolic profiling experiment consists of several steps of which the analytical GC–MS/LC–MS step is preceded by a sample preparation stage. This is also a critical step for a successful outcome of a metabolite profiling experiment (Villas-Boâs and Bruheim 2007). For microbial and cell culture systems many metabolites have a rapid turnover implying that the quenching of the metabolism should occur in less than a second. This is technically challenging and the most frequently used quenching solution is cold (i.e., <-40 °C) methanol–water solution, but acids have also been used. At this stage, it is preferable to separate intact biomass from the medium. However, it has been difficult to develop quenching protocols that leave the cells intact thereby preventing metabolite leakage (van Gulik 2010; Winder et al. 2008). The latest modification of the yeast quenching method, lately adjusted to *Pichia pastoris*, reports no leakage prior to the extraction step (Canelas et al. 2008; Carnicer et al. 2012), but this protocol does not prevent leakage of metabolites when applied to bacterial cells. Differential approaches where the quenched cell suspension is compared to the cell free supernatant control have been introduced in order to check for leakage (Winder et al. 2008). By contrast, rapid filtration is frequently used for analysis of metabolite groups with longer turnover rates, e.g. amino acids and non-amino organic acids (Meyer et al. 2010). Nevertheless, the metabolomics methodologies are continuously developing, in parallel with metabolite profiling reports giving new and interesting knowledge about the different biological systems under study (Kvitvang et al. 2011; Lien et al. 2012).

Pseudomonas bacteria have not been subjected to many metabolome studies even though this bacterial genus represents important human pathogens (*P. aeruginosa*), is used as cell factory (*P. putida*), and as biocontrol agent producers and plant commensals (*P. fluorescens*). Behrends and co-workers used an NMR-footprinting approach and reported that MucA modulates osmotic stress tolerance in

P. aeruginosa (*Behrends* et al. 2010). Planktonic and biofilm modes of growth of *P. aeruginosa* has also been compared by NMR footprinting and fingerprinting, and chemical differences between these two types of cells have been reported (Gjersing et al. 2007). Frimmersdorf and coworkers used GC–MS and reported that metabolite patterns, not unexpectedly, were defined by growth condition but that the core metabolism *P. aeruginosa* was not that strongly influenced by growth phase, carbon source or genetic background (both WT and mucoid strains were analyzed) (Frimmersdorf et al. 2010). The probably most comprehensive metabolome study of any *Pseudomonas* species to date was performed by van der Werf et al. (2008). They used two GC–MS methods and one LC–MS method to explore the metabolome of *P. putida* grown on four different carbon sources.

Here we report a quantitative metabolic profiling study comparing an alginate producing *P. fluorescens mucA*- strain with several closely related non-producing strains. In the alginate producing strain, up to 60 % of the carbon is channeled to alginate synthesis indicating that major redistribution of intracellular metabolite fluxes must occur when *P. fluorescens* is switching from non-alginate to alginate production. Glycerol has become a very cheap industrial carbon source since it is a bi-product in biodiesel production, and was thus included as carbon source in addition to the more commonly used carbon source fructose. We chose to use both GC–MS and LC–MS/MS to cover important metabolite groups such as amino acids, organic acids, sugar phosphates and other phosphometabolites as well as nucleotides.

2 Materials and methods

2.1 Strains and cultivation conditions

For detailed description of strain constructions and cultivation conditions, refer to Borgos et al. (2012). In short, continuous cultivations were run in 3 L-Applicon bioreactors with an operating volume of 750 mL and a dilution rate of 0.04 h^{-1} using a defined minimal medium with either fructose or glycerol as carbon source. Sampling for metabolite analysis was performed at nitrogen limited steady-state conditions obtained after five volume changes at an average OD_{660} of 8.0 and dry weight 2.9 g/L. Five bacterial strains were used in this study; the *P. fluorescens* SBW25 wild-type and four mutants derived thereof: *mucA*-, *mucA*- Δ*algC*, Δ*algC*, and *mucA*- TT*algD* (TT: transcription terminator). Only the *mucA*- strain produces alginate and the three non-producing mutants serve as control strains for comparing the alginate non-producing wild type strain with the alginate producing *mucA*- strain.

2.2 Metabolite sampling and processing

The experimental design included two (*mucA*- Δ*algC* and Δ*algC* on fructose and all strains on glycerol) or three biological replicates (WT and *mucA*- on fructose) with four resamplings (sample preparation and analytical replicates) from each. Metabolite extracts were prepared using an adaptation of the cold methanol quenching and metabolite extraction technique described by other groups (de Koning and van Dam 1992; Villas-Bôas et al. 2005; Mashego et al. 2007; Winder et al. 2008). Two types of extracts were prepared: one for the LC–MS/MS analysis of metabolite classes with rapid turnover rates (i.e., sugar phosphates and nucleotides) and one for the GC–MS analysis focusing on amino acids and non-amino organic acids. The LC–MS/MS samples were prepared by quenching 2.0 mL of steady-state grown culture in 6.0 mL cold (−20 °C) 50 % methanol containing 100 µL of a internal standard mixture composed of 0.1 mM uniformly ^{13}C ^{15}N labelled AMP ($^{13}C_{10}$, $^{15}N_5$-AMP, Sigma-Aldrich) and 0.25 mM $^{13}C_1$-α-ketoisocaproic acid (Sigma-Aldrich) within a time frame of 5 s. After sampling the samples were stored at −80 °C awaiting sample work-up. Further processing involved extractions of metabolites through three freeze (liquid nitrogen)–thaw (−20 °C) cycles before a volume of 96 % ethanol (−20 °C) equal to the sample volume was added to the sample to precipitate alginate. The samples were then centrifuged at 15,000 rpm for 10 min (−15 °C) before a 1:2 dilution of the supernatant in de-ionized water (0 °C) was performed. Precipitation of lipids were performed by adding one part of cold chloroform (0 °C) to three parts of the cell-free supernatant before ethanol–methanol–water phase containing metabolites corresponding to 1 ml culture was frozen at −80 °C prior to freeze-drying (approximately 36 h).

The samples were reconstituted in 500 µL 60 % methanol prior to LC–MS/MS analysis. Cell-free supernatants were prepared as negative controls for differential analysis. GC–MS samples were prepared by rapid filtration of 2.0 mL steady-state grown culture through a stack of three filters (pore size diameters 1.2 µm (VWR cat# SART 11403-47-N), 0.8 µm (Millipore cat#AAWP04700), and 0.6 µm (VWR cat# SART 13005-47-N)). The filters were washed with 5.0 mL 3 % NaCl at ambient temperature before they were transferred to 8.0 mL −20 °C 37.5 % methanol containing 50 µL of a 0.8 mM d4-succinate, 0.4 mM d8-valine and 0.8 mM d3-alanine (Sigma-Aldrich) mixture as internal standards. The sampling was performed within a timeframe of 30 s. The samples were then subjected to the same procedure as the LC–MS/MS samples to produce metabolite extract samples corresponding to 1.0 mL of culture. The samples were reconstituted in 380 µL 1 M NaOH spiked

with 20 µL 1 mM d5-glutamate upon derivatization for GC–MS analysis.

2.3 LC–MS and GC–MS analysis

LC–MS/MS analysis was based on the method introduced by Luo et al. (2007) and performed on an Agilent 1200 series LC connected via an electrospray ion source to an Agilent 6410 triple quadrupole MS instrument. Forty-two common phosphorous containing metabolites were included in this MS/MS method and collision energies were optimized for each individual metabolite. For the LC–MS/MS analysis, within sequence variability was evaluated by quantification of internal standards added to the samples at the time of sampling. The average relative standard deviation of the mean (STDOM) of the two internal standards over all LC–MS sequences was 4 %. This indicates that negligible variation is introduced during sample preparation and by LC–MS/MS instrumental drift, making the direct conversion of response to concentration using external standards included in the LC–MS sequence justifiable. For the metabolite extracts from the five conditions with two biological replicas (*mucA*- Δ*algC* and Δ*algC* on fructose and all strains on glycerol) the average relative uncertainty in the weighted average of the mean for all detected metabolites was 6 %. For the three biological replica of *WT* grown on fructose and the three biological replica of *mucA*- grown on fructose the average relative uncertainty in the weighted average of the mean was 4 %. Because both two and three biological replica gave an average relative uncertainty close to the uncertainty expected for within sequence variability (the average relative STDOM of the internal standards) it was decided not to include three biological replicas for all conditions.

GC–MS analysis was performed on an Agilent 7890 GC-5975 MS instrument. The methyl chloroformate derivatization (MCF) procedure described by Villas-Bôas and co-workers was employed with double volumes (Smart et al. 2010; Villas-Boâs et al. 2003). An Agilent DB-5MS+DG column with length 30 m + 10 duraguard, inner diameter 0.250 mm and film thickness 0.25 µm was used. The oven temperature was kept at 45 °C for 2 min before a temperature gradient of 10 °C/min was employed until 300 °C was reached. The oven was then kept at 300 °C for 7.5 min. 2 µl sample were injected in pulsed splitless mode and the GC was operated in constant pressure (about 1 bar) mode using d5-glutamic acid (Sigma-Aldrich) for retention time locking at 16.52 min. The MS was set to scan from 50 *m/z* to 550 *m/z*. Data analysis was done using Agilent Deconvolution Reporting Software (DRS) with a custom made library. The library consists of 25 known metabolites and 123 unknowns (the unknowns are major unidentified peaks detected in representative chromatograms during preliminary experiments and were included in the library for monitoring potential variation between the different strains). For the GC–MS analysis, within sequence variability was evaluated by quantification of the three internal standards added to the samples at the time of sampling and one internal standard added to the samples prior to derivatization (d5-glutamic acid). Averaged over all GC–MS sequences relative STDOM for the three internal standards added at the time of sampling was 3 % and the average relative STDOM for the internal standard added prior to derivatization was 3 %. To normalize responses, four samples from a reference fermentation were included in each GC–MS sequence. This allowed normalization of the dataset to a reference state for which standard curves for conversion of responses to concentration was available. The average relative uncertainty in the weighted average of the mean for all metabolites detected by the GC–MS method was similar to the average relative uncertainty in the weighted average of the mean obtained with the LC–MS/MS method: 4 % for the four conditions with two biological replicas and 3 % for the two conditions with three biological replicas.

Concentrations of metabolites in nmol per gram dry weight cells (nmol/gDW) for the different strains on the two different carbon sources are provided in Supplementary Tables S1 and S2. The concentrations provided are weighted averages of biological replicates, with uncertainties calculated based on the STDOM for each replica (Taylor 1997).

3 Results

3.1 Experimental design and cultivation data

Two main biological topics are addressed in this study: the changes in metabolite pool composition associated with induction of alginate biosynthesis, and the metabolite pool adjustments made when utilizing different carbon sources. Cultivations were performed with either fructose or glycerol to study the carbon source dependence. A non-alginate producing *P. fluorescens* SBW25 wild type and an alginate producing *mucA*- mutant were used to compare the non-producing and alginate producing phenotype. In addition, several control strains were included in the study because lack of the anti-sigma factor MucA is known to lead to pleiotropic effects (Firoved and Deretic 2003). A *mucA*-Δ*algC* double mutant and a Δ*algC* single deletion mutant were used as non-alginate producing control strains for the fructose cultivations. The former harbors the *mucA* inactivation but does not produce alginate because precursor synthesis is halted by *algC* deletion. The Δ*algC* mutant serves as an additional control. A *mucA*- TT*algD* (TT:

transcription terminator) double mutant was used as a non-alginate producing *mucA*- control for the glycerol cultivations. This *mucA*- mutant is not able to produce alginate since most biosynthetic enzymes required for alginate production are not expressed due to inactivation of P_{algD}.

The strains were grown in continuous cultivations (chemostats) with a dilution rate of 0.04 h^{-1} and sampling was performed at steady state nitrogen-limited conditions. The cell mass concentrations were, as expected for nitrogen limited cultures, almost the same for all cultivations. However the carbon source consumption rates varied for the different strains, and especially the increased carbon source consumption rates for alginate producing strains are noteworthy (Table 1). The glycerol consumption rate was almost as high as the fructose consumption rate (on Cmole basis) for both WT and *mucA*- strains. The cell mass yield on carbon source (Y_{XS}) was, in general, rather low for bacteria indicating that a relatively high proportion of the carbon substrate goes towards cell maintenance possible because the cells are not experiencing carbon source limitation. Thus, they are not forced to use carbon at highest efficiency. If the proportion of the carbon source used for alginate production is excluded from the yield calculation (Y^{**}_{XS} for *mucA*- strains), the cell mass yield is significantly higher for the *mucA*- mutants, including the *mucA*- mutants not producing alginate (above 20 % for all *mucA*- single and double mutants in Table 1). This apparent improved cell synthesis capability of *mucA*- mutants should somehow be reflected in the metabolome of these mutants.

3.2 Initial evaluation of the metabolome data

Initially the metabolome data set was evaluated by principal component analysis (PCA). PCA is an unsupervised multivariate data analysis method used to aid interpretation through reduction of data dimensionality. The method identifies linear combinations of the original data variables thereby explaining data variability by a minimal number of PCs. Unscrambler X (CAMO ASA) was used for all PCAs with mean centered data scaled by dividing the variables by their standard deviation (STD). Figure 1a is the scores plot from a PCA of the entire metabolome data set with each point representing a biological replica. Each biological replica is the average of four technical replicas. The data swarm in Fig. 1a show four distinct groupings: the alginate producing strain on fructose (*mucA*- represented by blue circles), the non-alginate producing strains on fructose (WT, *mucA*- *ΔalgC* and *ΔalgC* represented by blue dots, blue squares and blue diamonds respectively), the alginate producing strain on glycerol (*mucA*- represented by red circles) and the non-alginate producing strains on glycerol (WT and *mucA*- TT*algD* represented by red dots and red stars respectively). The strongest separation along PC-1 is the separation of the alginate producing *mucA*- strain on glycerol from the three other groups, and the strongest separation along PC-2 is the separation of *mucA*- on fructose from the three other groups. The two groups closest together are the two groups composed of non-producing strains. The scores plot for a separate PCA of these two groups is shown in Fig. 1b. The PC-1 versus PC-2 plane separate the data swarm into three groups: the first group is WT and *ΔalgC* strains on fructose (blue dots and blue diamonds), the second group is *mucA*- *ΔalgC* on fructose (blue squares) and the third group is WT and *mucA*- TT*algD* on glycerol (red dots and red stars). PC-3 separates the non-alginate producing *mucA*- TT*algD* grown on glycerol from the *WT* grown on glycerol. The distinct groupings in Fig. 1a, b show that the metabolome data set contains information about *P. fluorescens* metabolism connected to whether it is using fructose or glycerol as carbon source, whether it is producing alginate or not, and whether *mucA* is inactivated or not. Loadings plot

Table 1 Measured and calculated cultivation data of *P. fluorescens* SBW25 wild type and mutants derived thereof

Carbon source	Strain	Carbon source uptake (mmolC/g DW h)	Acetylated alginate production (mmolC/g DW h)	CO_2 excretion (mmolC/g DW h)	Biomass production[a] (mmolC/g DW h)	Carbon balance (%)	Y_{XS} (%)	Y_{XS}[b] (%)
Fructose	SBW25	9.4	–	7.5	1.5	96	16	
	mucA-	18.3	13.1	4.6	1.5	104	8	29
	Δ*algC*	9.1	–	7.4	1.5	98	16	
	mucA- Δ*algC*	5.8	–	4.3	1.5	99	26	
Glycerol	SBW25	8.3	–	6.4	1.5	96	18	
	mucA-	17.5	11.8	3.6	1.5	97	9	26
	mucA- TT*algD*	6.9	–	5.0	1.5	95	22	

The table includes carbon source consumption rate and production rates of carbon containing compounds (i.e., acetylated alginate, CO_2 and biomass), percentage carbon recovery and yields (biomass/carbon source)

[a] Constant biomass composition is assumed

[b] This yield is based on carbon source consumption rate excluding carbon flux to alginate

corresponding to Fig. 1a, b can be found in Supplementary Fig. S1.

To investigate exactly what separates the alginate producing *mucA*- strain and the non-alginate producing *mucA*- *ΔalgC* and *mucA*- TT*algD* strains from the WT and *ΔalgC* strains, it is beneficial to do PCAs for the fructose and glycerol data separately to exclude variation introduced when utilizing different carbons sources. Figure 2 shows (a) the scores plot and (b) the loadings plot from a PCA of all cultivations on fructose (see Table 2 later in the text for an explanation of the abbreviations of metabolite names used in the loadings plot). The scores plot show three distinct groupings of the data swarm: *mucA*- (blue circles), WT and *ΔalgC* (blue dots and blue diamonds) and *mucA*- *ΔalgC* (blue squares). The scores plot and the loadings plot taken together show that *mucA*- has high levels of GMP, GDP and GDP-M, that WT and *ΔalgC* have high levels of ATP and Acetyl-CoA and that high levels of F1P, GAP, Suc and AMP seems to be in common for the *mucA*- and the *mucA*- *ΔalgC* strain. It is interesting to note that if two separate PCAs are done for the fructose data; one for the data collected by the LC–MS method and one for the data collected by the GC–MS method, the three groups of Fig. 2a show better separation on the scores plot of the LC–MS data than on the scores plot of the GC–MS data (Supplementary Fig. S2). This indicates that phosphometabolites and nucleotides are more affected by whether or not alginate is produced and by whether or not MucA is inactivated than amino and non-amino organic acids for cultivations on fructose. Figure 3 show (a) the scores plot and (b) the loadings plot from a PCA of all cultivations on glycerol. As for the fructose data, the scores plot for the glycerol data shows three distinct groupings: the alginate producing strain (*mucA*- represented by red circles), the non-alginate producing strain (WT represented by red dots) and the non-alginate producing *mucA*- mutant (*mucA*- TT*algD* represented by red stars). The loadings plot interpreted together with the scores plot show that the most distinctive feature for the *mucA*- strain is elevated levels of GMP, GDP, GDP-M, R5P, NAD, E4P, F1P, PEP and 3PG, the most distinctive feature for WT seems to be elevated levels of CTP, Glu, Orn, ATP and UTP and the most distinctive feature of *mucA*- TT*algD* seems to be elevated levels of Suc and Cit. As for the fructose data, separate PCAs of the glycerol LC–MS data and the glycerol GC–MS data showed that the LC–MS data better retains the separation of strains seen in Fig. 3a, again indication that phosphometabolites and nucleotides are more affected by alginate synthesis and *mucA* inactivation than amino acids and organic acids (Supplementary Fig. S3).

PCA of carbon source dependency is best analysed separately for alginate non-producing strains and the alginate producing strain because the variation between these two groups would otherwise dominate the analysis (as seen in Fig. 1, i.e. PCA of the non-alginate producing strains is given in Fig. 1b). Figure 4 shows the scores plot (a) and the

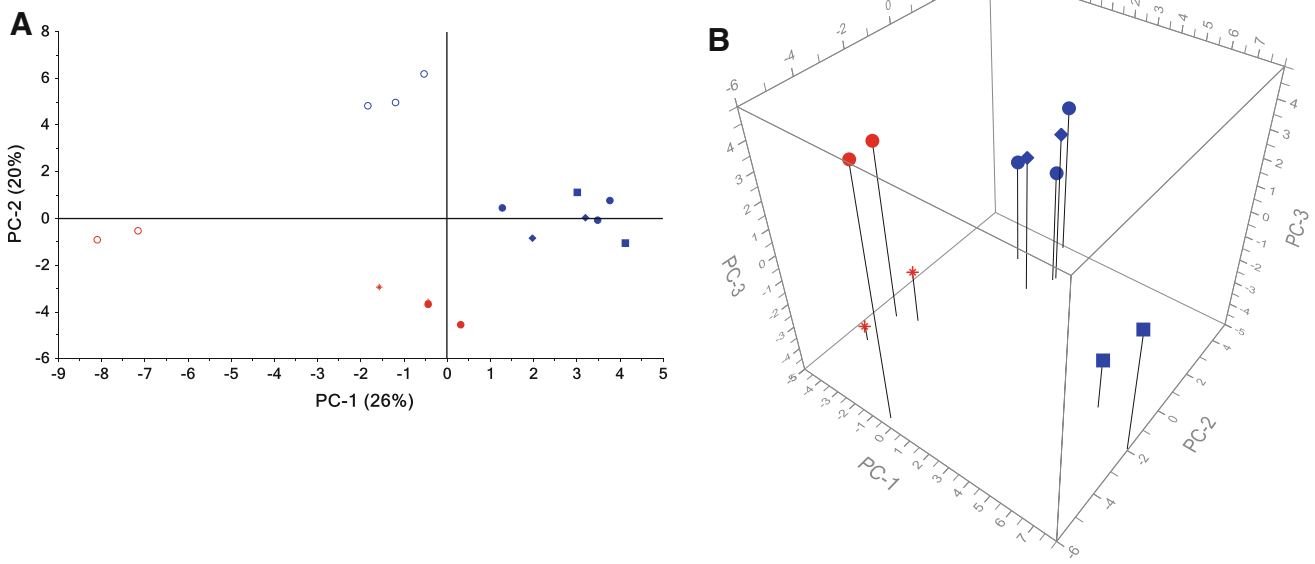

Fig. 1 **a** Scores plot from a PCA of the total metabolome data set (LC–MS and GC–MS data for both fructose and glycerol cultivations of all strains) and **b** scores plot from a PCA of the non-alginate producing strains for both fructose and glycerol cultivations. Each data point in the scores plot represents one biological replica. Corresponding loadings plot can be found in Supplementary Fig. S1. *Blue* fructose cultivations; *red* glycerol cultivations; *dots* wild type; *circles mucA*-; *squares mucA*- *ΔalgC*; *diamonds ΔalgC*; *stars mucA*- TT*algD*

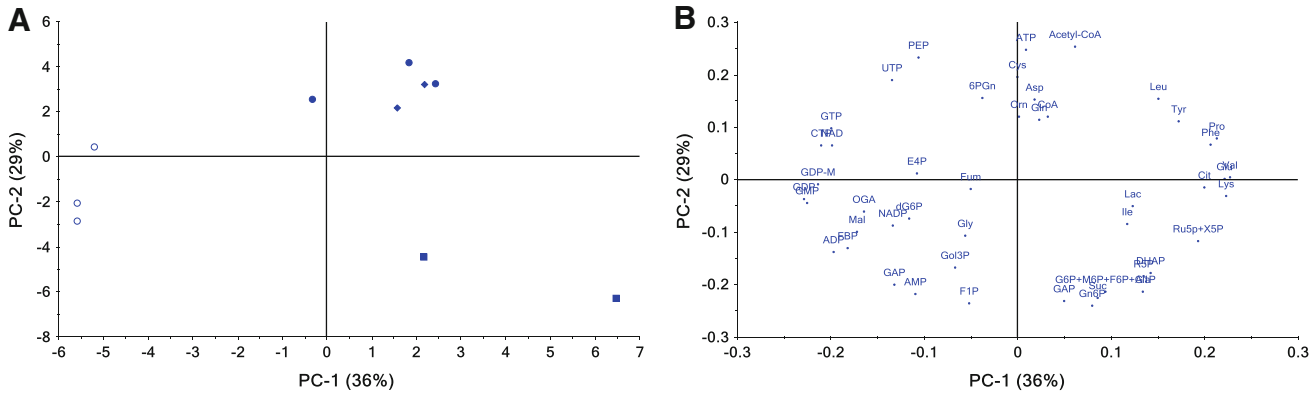

Fig. 2 **a** Scores plot and **b** loading plot of a PCA of the LC–MS and GC–MS data for cultivations on fructose. Each data point in the scores plot represents one biological replica. *Dots* wild type; *circles* *mucA*-; *squares mucA- ΔalgC*; *diamonds ΔalgC*. See Table 2 for an explanation of the abbreviations used and Supplementary Table S3 for numerical values for variables in the loadings plot

loadings plot (b) of a PCA of the *mucA*- strain grown on fructose and on glycerol. Two distinct groups have been separated along PC-1: *mucA*- grown on fructose (blue circles) and *mucA*- grown on glycerol (red circles). Interpretation of the scores plot and loadings plot together shows that growing *mucA*- on fructose leads to high concentrations of FBP, NADP and F1P and that growing *mucA*- on glycerol leads to high concentrations of Gol3P, DHAP, 3PG, R5P, PEP and 6PGn. PCAs were also performed separately for LC–MS and GC–MS data, and this showed that separation of strains and separation of a strain on different carbon sources are stronger for phosphometabolites and nucleotides than for amino acids and organic acids (Supplementary Figs. S4, S5).

The GC–MS library used for analysis included 123 unknowns in addition to 25 amino acids and organic acids. A separate PCA was performed for the unknowns to look for specific compounds that stood out in separating the various strains on the different carbons sources. The PCA showed some separation of strains but the loadings plot indicated that many unknown compounds contributed to this separation, and thus no limited number of unknown compounds were chosen for further investigation (see Supplementary Fig. S6 for PCAs of unknown compounds).

3.3 Comparison of metabolite pools of alginate producing and non-producing strains cultivated on fructose

Although a powerful multivariate data analysis technique, PCA does not yield quantitative information about the metabolic consequences of MucA inactivation, quantitative information about the metabolic changes associated with alginate production or quantitative information about metabolic adjustments connected to different carbons sources. Figures 5 and 6 give a semi-quantitative visualization of the metabolome data as color coded boxes presented in a metabolic network using the visualization software Omix (Droste et al. 2011). Figure 5 display results for fructose cultivations and Fig. 6 display results for glycerol cultivations. The metabolic pathways displayed are the glycolytic/Emden-Meyerhof Parnas pathway (EMP), the pentose phosphate pathway (PPP), the tricarboxylic acid pathway (TCA), the alginate biosynthetic pathway and the Entner-Doudoroff pathway (EDP) used by *Pseudomonas* (Conway 1992). Detected amino acids are also included in the network connected to their precursor metabolites. Metabolite concentrations are presented as ratios of mutants to WT using the weighted average of biological replica for each strain. The ratios are visualized by color interpolation from green (ratio of 0.13) to red (ratio of 8.00) on a logarithmic scale. For yellow boxes (ratio of 1.00) the metabolite concentration is equal for mutant and WT. As relative uncertainties for the ratios in most instances are below 10 % (see Supplementary Tables S4 and S5 for numerical value of ratios and corresponding uncertainties), detectable color differences in Figs. 5 and 6 generally represent significant differences between strains (the colors next to each other on the bottom right color scale of the figures differ by 41 %).

Looking at the fructose cultivations (Fig. 5) the mutant with the most WT-like metabolome is the Δ*algC* stain. This is expected as only one enzymatic activity, the phosphomannomutase, is inactivated in this mutant. The most notable observation for the Δ*algC* mutant is the fourfold decrease in concentration of GDP-M, presumably due to the mutant's reduced ability to produce the alginate precursor M1P. The concentration of GDP-M is even more decreased for the *mucA- ΔalgC* mutant: it is actually below the detection limit (grey box), whilst for *mucA*- GDP-M concentration is elevated compared to the WT strain. Comparing the two *mucA*- mutants to the WT, the most notable

Table 2 Absolute concentrations [nmol/gDW] of phosphometabolites, amino acids and organic acids given as weighted average (WAV) of biological replicates for *P. fluorescens* SBW25 wild type and *mucA*- mutant grown on fructose and glycerol provided with relative uncertainties (RU)

Metabolite	CID	Fructose				Glycerol			
		WT		*mucA*		WT		*mucA*	
		WAV (nmol/g DW)	RU (%)	WAV (nmol/g DW)	RU (%)	WAV (nmol/g DW)	RU (%)	WAV (nmol/g DW)	RU (%)
NAD	5,892	1,812	3	2,543	3	1,551	2	2,957	1
NADP	5,886	479	3	618	2	472	2	422	1
ATP	5,957	2,149	2	1,070	5	1,276	7	892	2
ADP	6,022	1,732	2	3,387	3	1,563	3	2,279	1
AMP	6,083	1,339	2	12,066	3	860	1	12,554	1
GTP	6,830	557	2	720	6	211	7	297	2
GDP	8,977	744	2	3,189	5	383	4	4,061	2
GMP	6,804	555	3	4,730	4	208	2	7,612	1
CTP	6,176	423	3	729	3	329	6	158	1
UTP	6,133	560	2	631	3	388	6	316	2
Fructose 1-phosphate (F1P)	65,246	3,165	3	29,008	3	ND	102	2	
Glycerol 3-phosphate (Gol3P)	754	2,900	3	3,560	4	15,858	2	15,474	1
GDP-Mannose (GDP-M)	18,396	348	2	1,284	3	69	2	2,027	2
Glucose-6-phosphate (G6P)	5,958								
Mannose-6-phosphate (M6P)	69,507								
Fructose-6-phosphate (F6P)	65,127								
Glucose-1-phosphate (G1P)	65,533	26,182	3	31,727	3	27,552	2	47,801	1
Fructose 1,6-bisphoshate (FBP)	10,267	776	1	1,929	6	152	14	385	4
Dihydroxyacetonephosphate (DHAP)	668	3,514	3	3,615	4	8,659	4	280,741	
Glyceraldehyde 3-phosphate (GAP)	729	ND	255	18	586	2	820	1	
3-Phosphoglycerate (3PG)	724	8,229	2	15,239	3	16,941	6	111,603	1
Phosphoenolpyruvate (PEP)	1,005	2,278	3	1,955	4	3,251	3	23,523	1
6-Phosphogluconate (6Pgn)	91,493	2,924	1	966	3	348	12	7,776	3
Ribulose 5-phosphate	439,184								
Xyluse 5- Phosphate (Ru5P, X5P)	441,187	2,377	3	1,535	3	982	1	2,559	1
Ribose 5-phosphate (R5P)	439,167	840	1	821	3	166	3	1,759	1
Erythrose 4-phosphate (E4P)	122,357	ND	784	0	ND	72	2		
Acetyl-CoA	444,493	531	4	297	18	28	9	327	1
CoA	6,816	100	6	89	11	33	9	74	12
Citrate (Cit)	311	5,693	1	5,240	1	5,449	2	5,019	2
2-Oxoglutarate (OGA)	51	2,503	3	2,487	1	2,873	4	2,761	3
Succinate (Suc)	1,110	21,373	8	24,365	8	19,205	15	19,300	17
Fumarate (Fum)	444,972	4,562	0	4,594	0	4,465	0	4,465	0
Malate (Mal)	525	399	4	580	8	276	4	281	4
Glycine (Gly)	750	2,231	1	2,167	1	2,288	1	2,077	3
Cysteine (Cys)	594	1,002	1	1,005	1	1,064	2	1,006	1
Phenylalanine (Phe)	994	2,914	0	2,738	0	2,877	0	2,858	0
Tyrosine (Tyr)	1,153	118	8	60	12	139	11	85	21
Lactate (Lac)	612	10,982	7	8,866	6	4,954	19	6,098	18
Leucine (Leu)	857	494	5	424	5	367	4	323	4
Valine (Val)	1,182	3,612	1	3,487	0	3,803	1	3,695	1
Alanine (Ala)	602	4,088	1	4,126	1	4,256	1	4,092	2
Aspartate (Asp)	424	3,299	1	3,207	1	3,105	1	3,168	1
Lysine (Lys)	866	3,503	1	3,175	1	3,452	2	3,043	1

Table 2 continued

Metabolite	CID	Fructose				Glycerol			
		WT		*mucA*		WT		*mucA*	
		WAV (nmol/g DW)	RU (%)	WAV (nmol/g DW)	RU (%)	WAV (nmol/g DW)	RU (%)	WAV (nmol/g DW)	RU (%)
Isoleucine (Ile)	791	848	4	833	3	827	3	782	2
Glutamate (Glu)	611	59,437	5	29,711	7	45,772	7	32,621	7
Ornithine (Orn)	389	4,136	2	4,034	1	4,081	0	4,144	1
Glutamine (Gln)	738	5,064	6	5,586	7	2,949	6	4,353	16
Proline (Pro)	614	2,956	1	2,845	1	2,935	1	2,805	1

CID PubChem Compound IDentifier

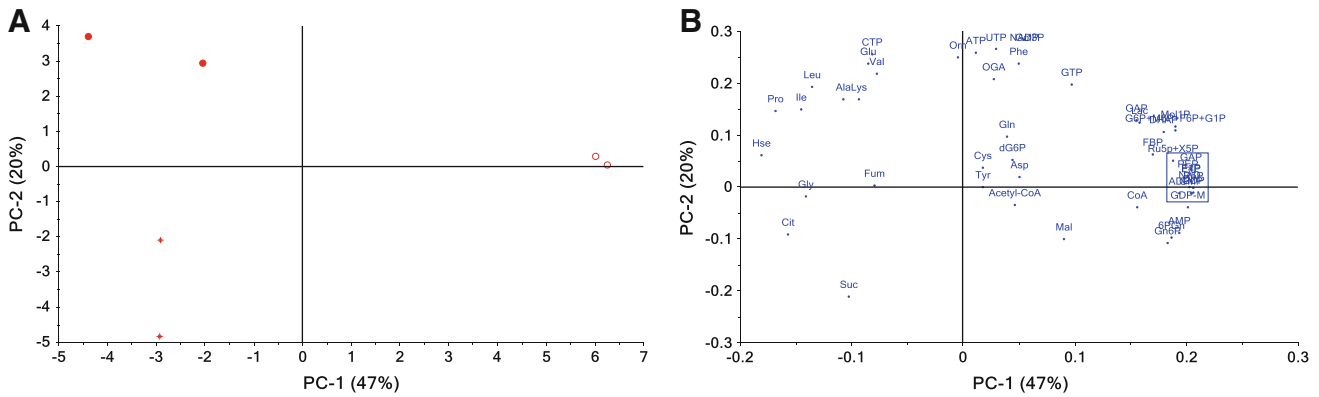

Fig. 3 **a** Scores plot and **b** loading plot of a PCA of the LC–MS and GC–MS data for cultivations on glycerol. Each data point in the scores plot represents one biological replica. In the loadings plot the metabolites GMP, GDP, GDP-M, R5P, NAD, E4P, F1P, PEP and 3PG are enclosed by a rectangle. *Dots* wild type; *circles mucA*-; *stars mucA*- TT*algD*. See Table 2 for an explanation of the abbreviations used and Supplementary Table S3 for numerical values for variables in the loadings plot

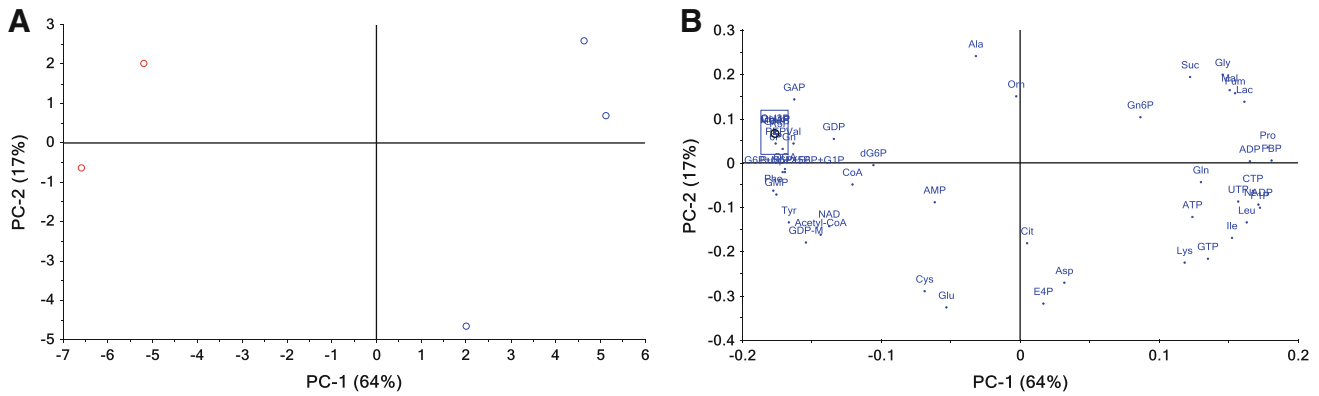

Fig. 4 **a** Scores plot and **b** loading plot of a PCA of LC–MS and GC–MS data for *mucA*- grown on both fructose (*blue*) and glycerol (*red*). Each data point in the scores plot represents one biological replica. In the loadings plot the metabolites Gol3P, 3PG, R5P, PEP and 6PGn are enclosed by a *rectangle*. See Table 2 for an explanation of the abbreviations used and Supplementary Table S3 for numerical values for variables in the loadings plot

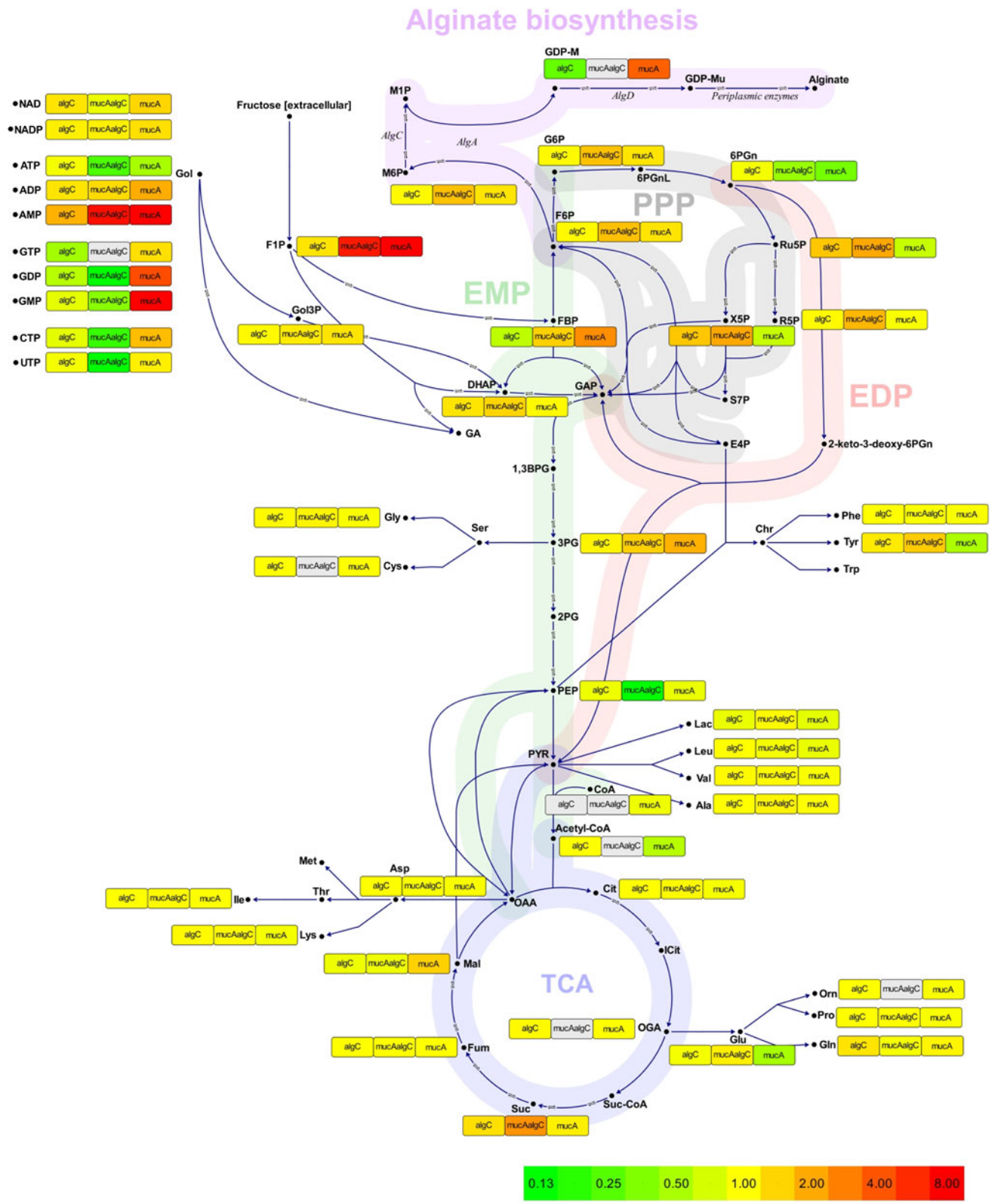

Fig. 5 Metabolome data from fructose cultivations visualized as color coded boxes of ratios of Δ*algC*, *mucA*- Δ*algC* and *mucA*-mutants relative to *P. fluorescens* SBW25 WT. The ratios have been *color* coded on a logarithmic scale as indicated on the bottom right bar. *Grey boxes* indicate a concentration below the detection limit. See Table 2 for an explanation of the abbreviations used

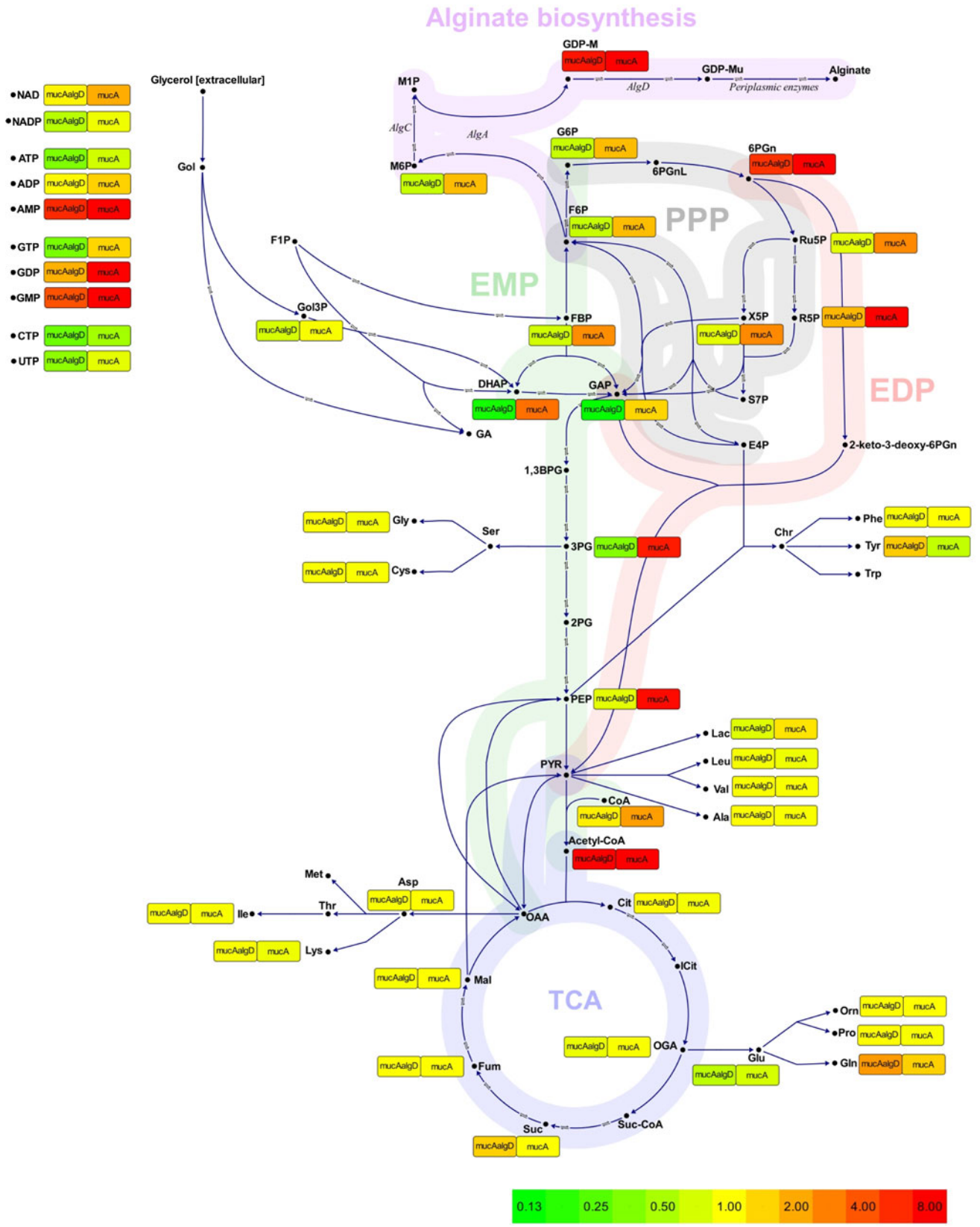

Fig. 6 Metabolome data from glycerol cultivations visualized as color coded boxes of ratios of *mucA*- TT*algD* and *mucA*- mutants relative to *P. fluorescens* SBW25 WT. The ratios have been *color* coded on a logarithmic scale as indicated on the bottom right bar. *Grey boxes* indicate a concentration below the detection limit. Table 2 for an explanation of the abbreviations used

differences are observed in the nucleotide pool. The *mucA-* and *mucA-* Δ*algC* mutants show the same pattern in the AXP pools (X: T, D, M) with lower concentration of ATP and higher concentrations of ADP and AMP relative to the WT. For the GXP nucleotide series the alginate producing *mucA-* mutant has a slightly higher pool of GTP and significantly higher pools of GDP and GMP, while the non-alginate producing *mucA-* Δ*algC* mutant has decreased pools of GTP (below detection level), GDP and GMP relatively to the WT. Clearly there are separate effects on the nucleotide pools by GTP-consuming alginate synthesis and by inactivation of the MucA anti-sigma factor. The most noteworthy observations among the phosphorylated metabolites in the glycolytic pathway and the PPP are the decreased 6-phosphogluconate (6PGn) pool and the increased fructose-1-phosphate (F1P) pool and glyceraldehyde 3-phosphate pool (GAP, values not displayed in Fig. 5 because concentration for WT is below detection limit) for the *mucA-* mutants. For amino acids and organic acids the differences between strains are much smaller. The most significant differences are the two-fold decrease in glutamate and tyrosine concentration for the alginate producing *mucA-* mutant and the doubled concentration of succinate (Suc) for the *mucA-* Δ*algC* mutant.

Many of the observations from Fig. 5 coincide with the result from the PCA of the fructose data (Fig. 2): *ΔalgC* is the mutant strain most similar to the WT strain, concentrations of GDP, GMP and GDP-M are especially high for *mucA-*, high concentration of F1P, GAP and AMP are characteristic of both *mucA-* and *mucA-* *ΔalgC* and phosphometabolites and nucleotides are more affected by MucA inactivation and alginate production than amino acids and organic acids.

3.4 Comparison of metabolite pools of alginate producing and non-producing strains cultivated on glycerol

Comparing cultivations on glycerol (Fig. 6) with cultivations on fructose (Fig. 5), the most apparent similarities are the higher concentration of mono- and di-phosphate nucleotides in the alginate producing strain relative to the WT strain, and the less variable amino and organic acid concentrations across the various strains. It is also in common for both carbons sources that the most noticeable change in amino and organic acids is the decrease in glutamate and tyrosine pools when alginate is synthesized. In other respects the glycerol cultivations differ from the fructose cultivations: GDP and GMP pools were lower for the non-alginate producing *mucA-* mutant relative to the WT when grown on fructose, whilst the non-alginate producing *mucA-* mutant grown on glycerol, *mucA-* TT*algD* has a higher concentration than the WT. Another difference when utilizing glycerol is that *mucA-* *ΔalgC* cultivated on fructose had undetectable amounts of GDP-M, whilst in contrast *mucA-* TT*algD* grown on glycerol has an elevated GDP-M concentration. The elevated concentration of GDP-M for *mucA-* TT*algD* is surprising as inactivation of P_{algD} should prevent synthesis of AlgA needed for synthesis of M6P and GDP-M. Another difference is that it is specific for glycerol cultivations that glycolytic pathway and PPP metabolites pools generally are higher in the *mucA-* strain and lower in the *mucA-* TT*algD* strain relative to the WT. It is also specific for glycerol cultivations that glycerol as the sole carbon source supports elevated 6-phosphogluconate and acetyl-CoA pools for the *mucA-* mutants.

Several of the observations from Fig. 6 coincide with the result from the PCA of the glycerol data (Fig. 3): the PCA also indicated that the different strains have more similar amino acid and organic acid concentrations than phosphometabolite and nucleotide concentrations, and the PCA indicated that the *mucA-* strain had high concentration of GDP-M and several intermediates in the glycolytic pathway and in PPP.

3.5 Comparison of metabolite pools in fructose and glycerol grown *mucA-* mutants and WT

Metabolite concentrations for WT and the *mucA-* strain are given in Table 2 for further investigation of how *P. fluorescens* adopts to different carbon sources (the data is presented in a metabolic network as ratios of glycerol cultivations to fructose cultivations in Supplementary Fig. S7). A comparison of the metabolome of fructose and glycerol grown *P. fluorescens* cells reveal both strain and carbon source dependencies. The PPP metabolite pools were lower on glycerol compared to fructose when there is no alginate production (WT), and higher when alginate is produced (*mucA-*). This is also true for GDP-M. Furthermore, the hexose-phosphate pool is similar in WT on glycerol and fructose, while is seems that turning on the alginate production in the *mucA-* mutant results in a slightly elevated level of hexose-phosphates on glycerol compared to fructose. So for these metabolites the strains behave differently on different carbons sources. In contrast glycerol-3-phosphate (Gol3P) and the four three-carbon compounds of the glycolytic pathway [dihydroxyacetonephosphate (DHAP), GAP, 3-phosphoglycerate (3PG) and phosphoenolpyruvate (PEP)] are all present at elevated concentrations when glycerol is used as carbon source. Also fructose-1,6-bisphosphate (FBP) and F1P behave in a carbon source dependent manner rather than strain dependent: the pool is significantly lower for both WT and *mucA-* when the cells are grown on glycerol compared to fructose. For most amino acids it seems that

changing the carbons source has little effect: the concentrations are similar for both WT and *mucA*- on the two carbons sources. Also independent of carbons source is the high concentrations of 3PG, the hexose-phosphates, lactate (Lac), succinate and glutamate compared to other metabolites for both strains. Several of these results were also found when comparing glycerol cultivations with fructose cultivations by PCA (see Fig. 4 for *mucA*-).

4 Discussion

The presented results show that inactivation of *mucA* has significant effects on the composition of the *P. fluorescens* metabolome, both in the presence and absence of alginate synthesis. Cultivation data from the chemostats revealed that the growth yield on carbon source increased from 16 % for WT on fructose to 26 % in *mucA*- Δ*algC* on fructose concurrent with an almost 40 % decrease in the fructose consumption rate (Table 1). Since the final cell titer was approximately the same in these nitrogen limited cultivations, this implies that the *mucA* inactivation results in a cell that is much more efficient in synthesizing cell material as it uses less of the excessive carbon source and converts a higher fraction of it into cell mass. Transcriptome analysis from the same set of cultivations identified a significantly up-regulation of ribosomal genes and genes involved in energy generation, including a ATP synthase subunit and dehydrogenase genes in *mucA*- mutants, while expression of metabolic genes were not significantly altered (Borgos et al. 2012). The metabolic profiling study reported here provides further insights into the pleiotropic effects of *mucA* inactivation.

4.1 The *mucA* mutation leads to a significantly reduced energy charge

The energy charge (EC = (ATP + 0.5 * ADP)/(ATP + ADP + AMP)) was found to be 0.58 and 0.56 for WT grown on fructose and glycerol, respectively. The EC dramatically decreased in the *mucA*- mutants (0.17 and 0.13 for the *mucA*- mutant grown on fructose and glycerol, respectively, and 0.13 for the *mucA*- Δ*algC* mutant on fructose and 0.20 for *mucA*- TT*algD* mutant on glycerol, respectively) while the Δ*algC* mutant had EC 0.46 on fructose (see Supplementary Table S1 for concentration values used for EC calculations). EC of actively growing bacterial cells is expected to be higher than 0.8 and cells become metabolically inert when the EC drops below 0.5 (Chapman et al. 1971). Therefore, the recorded ECs in this study are unexpectedly low, especially for the *mucA*- mutants. van der Werf et al. (2008) also reported low EC values on some carbon sources for *Pseudomonas putida* S12 (i.e., 0.07 and 0.50 on glucose and gluconate respectively) and high values on some other carbon sources (i.e., 0.87 and 0.84 on fructose and succinate respectively) in batch fermentations. Furthermore, Barrette et al. (1988) reported EC values below 0.3 for *E. coli* and *P. aeruginosa* but the cells recovered easily when unleashed from the growth limitation. Clearly, the issue of absolute EC threshold and viability must be revisited. However, it is important to remember that the EC might differ between bacterial strains and also with cultivation conditions (un-limited growth in batch-cultures versus nutrient-limited growth in chemostats). In addition, sampling and analytical protocols are factors that also can influence the final recorded measurement. The cold methanol extraction protocol was used in this study. Bolton and co workers presented an overview of several microbial studies using this protocol, and showed that EC values varied from 0.16 to 0.92 in these studies (Bolten et al. 2007). Clearly, the development of a rapid inactivation protocol for bacteria without metabolite leakage with subsequent extraction of all metabolite groups has not yet been successful, even though many research groups have focused on this important aspect of metabolomics (Bolten et al. 2007; Taymaz-Nikerel et al. 2009; van Gulik 2010; Villas-Boâs and Bruheim 2007; Winder et al. 2008). Irrespective of this, on a relative basis, the metabolic profiling data presented in this study provide some important insight into the altered metabolism of *mucA*- mutants. The absolute concentrations presented in Table 2 show that it is predominantly the high concentration of AMP in the *mucA*- mutants that cause the EC reduction in these strains. A significantly increased AMP pool was also observed in the *P. putida* S12 glucose cultivation compared to the fructose cultivation (van der Werf et al. 2008), which indicate that *Pseudomonas* cell nucleotide pools are adjusted also by cultivations conditions in addition to changed genotype (i.e., *mucA* inactivation). The observation of lower ECs and higher growth yield on carbon source in *mucA*- mutants is quite surprising as a low EC should favor catabolism rather than anabolism. But, the results indicate that as long as the ATP pool is maintained above a critical level, the apparent low ECs does not impair growth capabilities. Also, glycerol is more reduced (i.e., more energy rich) but fructose supports higher ATP pools both in WT and *mucA*- implying that there is no direct correlation between ATP pool size and degree of reduction of the carbon substrate. On a relative basis, however, the cells are able to maintain similar EC values on the two different carbon sources showing that not only relative (i.e., EC) but also absolute concentrations of nucleotides are of importance for maintaining viability and growth performance.

4.2 Metabolite pools sizes are adjusted through increased carbon source consumption rates in alginate producing *mucA*- strain

The carbon source uptake is adjusted to cover the consumption related to alginate synthesis (Table 1). A reflection of this is seen in the overall picture of changes in the metabolite pools comparing alginate producing to non-producing cells; as the cells are growing with same growth rate and obtaining same dry weight concentration, the amino acid pool is less affected than the phosphometabolite and nucleotide pools. Frimmersdorf et al. (2010) working with shake flask batch cultures also observed minor changes in core metabolism metabolites between wild type and mucoid *P. aeruginosa* strains cultivated on different carbon sources. However, when interpreting metabolite pool data it is important to realize that there is no direct link between metabolite pool sizes and metabolic fluxes, although changes in metabolite pool sizes indicate that, and likely where, perturbations of the metabolic network have occurred. Substrate consumption rates and growth/production rates can to some extent guide the interpretation of the data when true intracellular metabolic flux distribution data is lacking, i.e., for glycerol cultivations there must be an increased metabolic flux from glycerol via GAP/DHAP to the alginate precursor metabolite F6P for the alginate producing *mucA*- mutant compared to WT. Interestingly, the higher PPP metabolite pools in *mucA*- mutant on glycerol must be a consequence of this increased flux from glycerol to F6P. However, it can not be concluded that there is an increased flux through the PPP for *mucA*- mutant on glycerol, and there is no obvious reason for the cell to increase the PPP flux since neither NADPH nor pentose phosphates are needed for alginate synthesis. But there seems to be a direct correlation between increased metabolic fluxes and increased pool sizes close to the carbon source entry site in the primary metabolic pathway since both F1P and FBP pools are increased in *mucA*- mutant on fructose, and 3PG, PEP and DHAP pools are increased in *mucA*- mutant on glycerol. Interestingly, the FBP pool is larger in the fructose—WT than the glycerol—*mucA*- cultivation (Table 2), even though the carbon flux from glycerol to alginate via FBP in *mucA*- mutant is of the same magnitude as the total fructose uptake rate in WT. Clearly, there is no direct and unambiguous link between metabolite concentration and metabolic flux.

4.3 Composition of GXP nucleotides is significantly changed in alginate producing cells

While the changes in AXP pools were attributed to the inactivation of *mucA*, the changes in GXP pools are attributed to activation of alginate synthesis. If fructose is used as carbon source two ATP is used to activate fructose to F6P via FBP and one GTP is used for synthesis of GDP-M. The two NADH produced in the oxidation of the latter metabolite to GDP-Mu by AlgD should therefore via oxidative phosphorylation and nucleoside di-phosphate kinases provide enough high-energy phosphates to support alginate synthesis without extra oxidation of fructose to CO_2 for additional energy formation. But, imposing alginate production increases the turnover rates in the GXP pools and the dramatic increased concentration of GDP and GMP indicate a strong cellular response to the increased GTP consumption.

In conclusion, the metabolite pool measurements constitute a complex picture of the relation between alginate synthesis and carbon and energy metabolism in *P. fluorescens*. The most significant findings in this study are the changes in GXP pools related to alginate synthesis and the changes in AXP pools related to *mucA* inactivation. Many minor, though interesting, findings on how *P. fluorescens* metabolite pools are adjusted to various conditions were also observed. More information about kinetics, regulation and metabolic flux distribution are needed to interpret the data further, especially to find out how inactivation of the anti-sigma factor *mucA* contribute to the increased growth yield.

Acknowledgments S.K.L., H.S., T.E.E, S.V., K.V., S.E.F.B. and P.B. would like to thank The Research Council of Norway for financial support. E.C. and R.G. would like to thank the Biotechnology and Biological Sciences Research Council, BBSRC for their financial support. The authors acknowledge the collaborators in the Era-net "Systems Biology of Microorganisms" SysMO project.

References

Barrette, W. C., Hannum, D. M., Wheeler, W. D., & Hurst, J. K. (1988). Viability and metabolic capability are maintained by *Escherichia coli*, *Pseudomonas aeruginosa*, and *Streptococcus lactis* at very low adenylate energy-charge. *Journal of Bacteriology, 170*, 3655–3659.

Behrends, V., Ryall, B., Wang, X. Z., Bundy, J. G., & Williams, H. D. (2010). Metabolic profiling of *Pseudomonas aeruginosa* demonstrates that the anti-sigma factor MucA modulates osmotic stress tolerance. *Molecular BioSystems, 6*, 562–569. doi:10.1039/b918710c.

Bolten, C. J., Kiefer, P., Letisse, F., Portais, J. C., & Wittmann, C. (2007). Sampling for metabolome analysis of microorganisms. *Analytical Chemistry, 79*, 3843–3849. doi:10.1021/ac0623888.

Borgos, S. E., et al. (2012). Mapping global effects of the transcription factor MucA in *Pseudomonas fluorescens* through genome-scale metabolic modeling. *BMC Genome Biology,* (submitted).

Canelas, A. B., Ras, C., ten Pierick, A., van Dam, J. C., Heijnen, J. J., & Van Gulik, W. M. (2008). Leakage-free rapid quenching technique for yeast metabolomics. *Metabolomics, 4*, 226–239. doi:10.1007/s11306-008-0116-4.

Carnicer, M., et al. (2012). Development of quantitative metabolomics for *Pichia pastoris*. *Metabolomics, 8*, 284–298. doi:10.1007/s11306-011-0308-1.

Chapman, A. G., Fall, L., & Atkinson, D. E. (1971). Adenylate charge in *Escherichia coli* during growth and starvation. *Journal of Bacteriology, 108*, 1072–1086.

Conway, T. (1992). The Entner-Doudoroff pathway—history, physiology and molecular-biology. *FEMS Microbiology Reviews, 103*, 1–28. doi:10.1016/0378-1097(92)90334-k.

de Koning, W., & van Dam, K. (1992). A method for the determination of changes of glycolytic metabolites in yeast on a subsecond time scale using extraction at neutral pH. *Analytical Biochemistry, 204*(1), 118–123.

Droste, P., Miebach, S., Niedenfuhr, S., Wiechert, W., & Noh, K. (2011). Visualizing multi-omics data in metabolic networks with the software Omix—a case study. *Biosystems, 105*, 154–161. doi:10.1016/j.biosystems.2011.04.003.

Ellis, D. I., & Goodacre, R. (2012). Metabolomics-assisted synthetic biology. *Current Opinion in Biotechnology, 23*, 22–28.

Firoved, A. M., & Deretic, V. (2003). Microarray analysis of global gene expression in mucoid *Pseudomonas aeruginosa*. *Journal of Bacteriology, 185*, 1071–1081. doi:10.1128/jb.185.3.1071-1081.2003.

Frimmersdorf, E., Horatzek, S., Pelnikevich, A., Wiehlmann, L., & Schomburg, D. (2010). How *Pseudomonas aeruginosa* adapts to various environments: a metabolomic approach. *Environmental Microbiology, 12*, 1734–1747. doi:10.1111/j.1462-2920.2010.02253.x.

Gjersing, E. L., Herberg, J. L., Horn, J., Schaldach, C. M., & Maxwell, R. S. (2007). NMR metabolomics of planktonic and Biofilm modes of growth in *Pseudomonas aeruginosa*. *Analytical Chemistry, 79*, 8037–8045. doi:10.1021/ac070800t.

Hassett, D. J., Sutton, M. D., Schurr, M. J., Herr, A. B., Caldwell, C. C., & Matu, J. O. (2009). *Pseudomonas aeruginosa* hypoxic or anaerobic biofilm infections within cystic fibrosis airways. *Trends in Microbiology, 17*, 130–138. doi:10.1016/j.tim.2008.12.003.

Hay, I. D., Rehman, Z. U., Ghafoor, A., & Rehm, B. H. A. (2010). Bacterial biosynthesis of alginates. *Journal of Chemical Technology and Biotechnology, 85*, 752–759. doi:10.1002/jctb.2372.

Kvitvang, H. F. N., Andreassen, T., Adam, T., Villas-Boâs, S. G., & Bruheim, P. (2011). Highly sensitive GC/MS/MS method for quantitation of amino and nonamino organic acids. *Analytical Chemistry, 83*, 2705–2711. doi:10.1021/ac103245b.

Lien, S. K., Kvitvang, H. F., & Bruheim, P. (2012). Utilization of a deuterated derivatization agent to synthesize internal standards for gas chromatography–tandem mass spectrometry quantification of silylated metabolites. *Journal of Chromatography A,*. doi:10.1016/j.chroma.2012.05.053.

Lu, W., Bennett, B. D., & Rabinowitz, J. D. (2008). Analytical strategies for LC-MS-based targeted metabolomics. *Journal of Chromatography B-Analytical Technologies in the Biomedical and Life Sciences, 871*, 236–242. doi:10.1016/j.jchromb.2008.04.031.

Luo, B., Groenke, K., Takors, R., Wandrey, C., & Oldiges, M. (2007). Simultaneous determination of multiple intracellular metabolites in glycolysis, pentose phosphate pathway and tricarboxylic acid cycle by liquid chromatography-mass spectrometry. *Journal of Chromatography A, 1147*, 153–164. doi:10.1016/j.chroma.2007.02.034.

Martin, D. W., Schurr, M. J., Mudd, M. H., Govan, J. R. W., Holloway, B. W., & Deretic, V. (1993). Mechanism of conversion to mucoidy in *Pseudomonas aeruginosa* infecting cystic-fibrosis patients. *Proceedings of the National academy of Sciences of the United States of America, 90*, 8377–8381. doi:10.1073/pnas.90.18.8377.

Mashego, M. R., Rumbold, K., de Mey, M., Vandamme, E., Soetaert, W., & Heijnen, J. J. (2007). Microbial metabolomics: past, present and future methodologies. *Biotechnology Letters, 29*(1), 1–16.

Meyer, H., Liebeke, M., & Lalk, M. (2010). A protocol for the investigation of the intracellular *Staphylococcus aureus* metabolome. *Analytical Biochemistry, 401*, 250–259. doi:10.1016/j.ab.2010.03.003.

Nielsen, J., & Oliver, S. (2005). The next wave in metabolome analysis. *Trends in Biotechnology, 23*, 544–546. doi:10.1016/j.tibtech.2005.08.005.

Rehm, B. H. A. (2010). Bacterial polymers: biosynthesis, modifications and applications. *Nature Reviews Microbiology, 8*, 578–592. doi:10.1038/nrmicro2354.

Schnider-Keel, U., Lejbolle, K. B., Baehler, E., Haas, D., & Keel, C. (2001). The sigma factor AlgU (AlgT) controls exopolysaccharide production and tolerance towards desiccation and osmotic stress in the biocontrol agent *Pseudomonas fluorescens* CHA0. *Applied and Environmental Microbiology, 67*, 5683–5693. doi:10.1128/aem.67.12.5683-5693.2001.

Smart, K. F., Aggio, R. B. M., Van Houtte, J. R., & Villas-Boâs, S. G. (2010). Analytical platform for metabolome analysis of microbial cells using methyl chloroformate derivatization followed by gas chromatography-mass spectrometry. *Nature Protocols, 5*, 1709–1729. doi:10.1038/nprot.2010.108.

Sumner, L. W., et al. (2007). Proposed minimum reporting standards for chemical analysis. *Metabolomics, 3*, 211–221. doi:10.1007/s11306-007-0082-2.

Taylor, J. R. (1997). *7.2 The weighted average. An introduction to error analysis* (2nd ed., pp. 174–176). Sausalito, USA: University Science Books.

Taymaz-Nikerel, H., et al. (2009). Development and application of a differential method for reliable metabolome analysis in *Escherichia coli*. *Analytical Biochemistry, 386*, 9–19. doi:10.1016/j.ab.2008.11.018.

van der Werf, M. J., Overkamp, K. M., Muilwijk, B., Coulier, L., & Hankemeier, T. (2007). Microbial metabolomics: Toward a platform with full metabolome coverage. *Analytical Biochemistry, 370*, 17–25. doi:10.1016/j.ab.2007.07.022.

van der Werf, M. J., et al. (2008). Comprehensive analysis of the metabolome of *Pseudomonas putida S12* grown on different carbon sources. *Molecular BioSystems, 4*, 315–327. doi:10.1039/b717340g.

van Gulik, W. M. (2010). Fast sampling for quantitative microbial metabolomics. *Current Opinion in Biotechnology, 21*, 27–34. doi:10.1016/j.copbio.2010.01.008.

Villas-Boâs, S. G., & Bruheim, P. (2007). The potential of metabolomics tools in bioremediation studies. *Omics—A Journal of Integrative Biology, 11*, 305–313. doi:10.1089/omi.2007.0005.

Villas-Boâs, S. G., & Bruheim, P. (2007). Cold glycerol-saline: The promising quenching solution for accurate intracellular metabolite analysis of microbial cells. *Analytical Biochemistry, 370*, 87–97. doi:10.1016/j.ab.2007.06.028.

Villas-Boâs, S. G., Delicado, D. G., Akesson, M., & Nielsen, J. (2003). Simultaneous analysis of amino and nonamino organic acids as methyl chloroformate derivatives using gas chromatography-mass spectrometry. *Analytical Biochemistry, 322*, 134–138. doi:10.1016/j.ab.2003.07.018.

Villas-Boâs, S. G., Moxley, J. F., Åkesson, M., Stepanopolous, G., & Nielsen, J. (2005). High-throughput metabolic state analysis: the missing link in integrated functional genomics of yeasts. *Biochemical Journal, 388*, 669–677.

Wentzel, A., Sletta, H., Consortium, S., Ellingsen, T. E., & Bruheim, P. (2012). Intracellular metabolite pool changes in response to nutrient depletion induced metabolic switching in *Streptomyces coelicolor*. *Metabolites, 2*, 178–194. doi:10.3390/Metabo2010178.

Winder, C. L., et al. (2008). Global metabolic profiling of *Escherichia coli* cultures: An evaluation of methods for quenching and extraction of intracellular metabolites. *Analytical Chemistry, 80*, 2939–2948. doi:10.1021/ac7023409.